JACS
JOURNAL OF THE AMERICAN CHEMICAL SOCIETY
Article
pubs.acs.org/JACS

Probing the Magic Numbers of Aluminum−Magnesium Cluster Anions and Their Reactivity toward Oxygen

Zhixun Luo,[†,§] Cameron J. Grover,[‡,§] Arthur C. Reber,[‡] Shiv N. Khanna,*[,‡] and A. W. Castleman, Jr.*[,†]

[†]Departments of Chemistry and Physics, The Pennsylvania State University, University Park, Pennsylvania 16802, United States
[‡]Department of Physics, Virginia Commonwealth University, Richmond, Virginia 23284, United States

Supporting Information

ABSTRACT: We report a joint experimental and theoretical investigation into the geometry, stability, and reactivity with oxygen of alloy metal clusters $Al_nMg_m^-$ ($4 \le n+m \le 15$; $0 \le m \le 3$). Considering that Al and Mg possess three and two valence electrons, respectively, clusters with all possible valence electron counts from 11 to 46 are studied to probe the magic numbers predicted by the spherical jellium model, and to determine whether enhanced stability and reduced reactivity may be found for some $Al_nMg_m^-$ at non-magic numbers. $Al_5Mg_2^-$ and $Al_{11}Mg_3^-$ exhibit enhanced stability corresponding to the expected magic numbers of 20 and 40 electrons, respectively; while $Al_7Mg_3^-$, $Al_{11}Mg^-$, and $Al_{11}Mg_2^-$ turn out to be unexpectedly stable at electron counts of 28, 36, and 38, respectively. The enhanced stability at non-magic numbers is explained through a crystal-field-like splitting of degenerate shells by the geometrical distortions of the clusters. $Al_nMg_m^-$ clusters appear to display higher oxidation than pure Al_n^- clusters, suggesting that the addition of Mg atoms enhances the combustion of pure aluminum clusters.

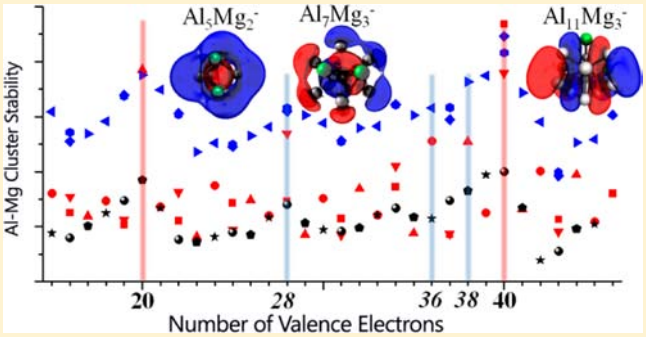

1. INTRODUCTION

Aluminum oxidizes with the second largest heat of combustion per volume of all the elements; however, it is generally coated with an oxide "dead" layer which impedes its application as an energetic material.[1−3] Magnesium is also prone to corrosion and is covered with an oxide or hydroxyl layer when exposed to air and moisture. Metal alloys composed of aluminum and magnesium have been widely recognized to be of importance in industry and aerospace manufacturing, as they are not only cheaper and lighter than other aluminum alloys but also less flammable than other alloys that contain a high percentage of magnesium. It is interesting to note that the addition of a few percent of aluminum along with zinc enhances the corrosion resistance of bulk magnesium.[4]

In the nanoscale regime, aluminum clusters exhibit variable reactivity, with some clusters bearing remarkable resistance to the reactivity with O_2.[5−13] The reactivity of such clusters is generally explained by the valence electron count, where the clusters with a "magic" number of electrons have enhanced stability. Each aluminum atom has 3 valence electrons, and magnesium has 2 valence electrons. This means that, by examining $Al_nMg_m^-$ clusters at $4 \le n+m \le 15$ and $0 \le m \le 3$, we are able to investigate the stability and electronic structures of the clusters with all possible valence electron counts from 11 to 46 so as to test the limits of the magic numbers in aluminum-based alloy clusters.

Nearly 30 years ago, Castleman and co-workers[5] observed that selected small aluminum cluster anions (Al_{13}^-, Al_{23}^-, and Al_{37}^-) were highly resistant to oxidation, which enables a pathway to attain cluster-assembled materials free of a "dead" layer of oxide.[15,16] Theoretical studies found that the novel behavior is due to the quantum confinement of the nearly free-electron gas (NFEG) leading to a grouping of electronic states into shells.[6] A spherical jellium model wherein the ionic cores are replaced by a uniform positive background provides a simplified model in which the electronic states order as 1S, 1P, 1D, 2S, 1F, ... shells.[17] [All the characters like 1S, 1P, 1D, etc. refer to such orbitals.] Therefore, clusters with a magic number of electrons, 2, 8, 18, 20, 34, 40, ..., have closed electronic shells and enhanced stability. Note that the jellium model assumes the clusters to be spherical, which may be a poor approximation in some cases. In general, clusters with fully filled electronic shells have large gaps between the highest occupied molecular orbitals (HOMOs) and lowest unoccupied molecular orbitals (LUMOs), and they are generally resistant to oxidation by O_2.[6] This is because the ground state of an oxygen molecule is spin triplet, and any activation of the molecule requires a filling of the minority states. For clusters with fully filled electronic shells, the angular momentum conservation requires a spin excitation of the cluster.

Our recent studies on Al_nCu^- alloy metal clusters[18] found that geometrical distortions can lead to splitting of the shells in the spherical jellium, and this splitting can be intuitively

Received: October 23, 2012
Published: February 23, 2013

   dx.doi.org/10.1021/ja310467n | J. Am. Chem. Soc. 2013, 135, 4307−4313

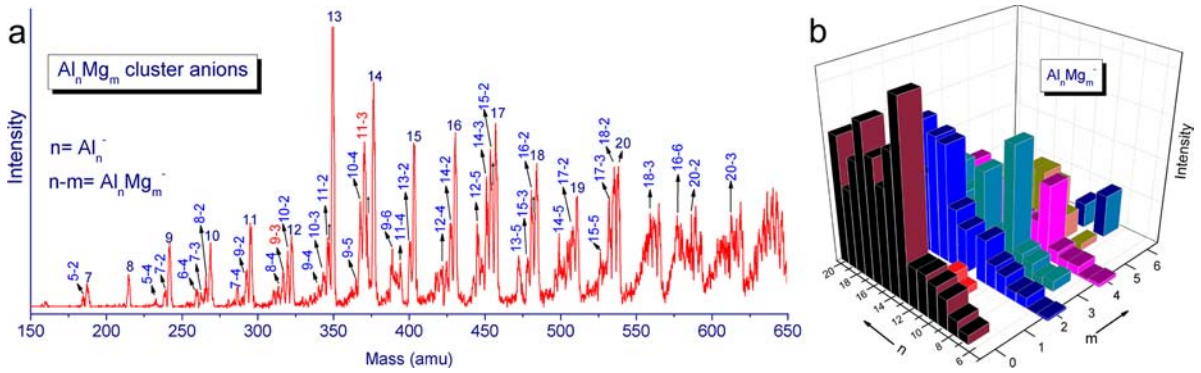

Figure 1. (a) Representative size distribution of the observed $Al_nMg_m^-$ cluster anions, where the indicated numbers (n and $n-m$) correspond to $Al_nMg_m^-$ ($0 \le m \le 6$). (b) Three-dimensional histograms of the integral signal intensities of the observed $Al_nMg_m^-$ clusters.

understood as a crystal-field-like splitting of the electronic shells.[19] Among these Al_nCu^- species, the clusters with fully filled subshells and large HOMO−LUMO gaps are found to be resistant to oxidation, supporting the idea that spin excitations hold the key in their reactivity with oxygen. Could these ideas be extended to aluminum−magnesium clusters? Since magnesium is divalent while aluminum is trivalent, the alloy clusters offer larger variations over the electron counts than pure aluminum clusters and hence provide more rigorous grounds to examine the underlying principles.

In the present study, we explore the structures, stability, and electronic character of small aluminum−magnesium clusters containing up to 15 atoms. Our approach combines first-principles calculations with experiments employing a flow tube reactor coupled with mass spectrometry. Experiments were made for a range of distributions of $Al_nMg_m^-$ species, with results displayed for several clusters revealing resistance to oxygen etching. The experimental observations accord well with the theoretical prediction. We identify the alloy clusters[20−30] that are stabilized by having a magic number of electrons corresponding to a spherical closed shell, such as $Al_5Mg_2^-$ and $Al_{11}Mg_3^-$ with 20 and 40 valence electrons, respectively. We also distinguish clusters with enhanced stability that have non-magic numbers of valence electrons, such as $Al_7Mg_3^-$, $Al_{11}Mg^-$, and $Al_{11}Mg_2^-$, whose stability is due to the splitting of subshells related to their geometric structures. These findings on stable $Al_nMg_m^-$ species indicate the potential in forming cluster-assembled materials of the Al−Mg alloy with corrosion resistance when exposed to external aerobic environment, and enable a test of the limits and useful modifications of the jellium model.[31−34]

2. EXPERIMENTAL AND THEORETICAL METHODS

2.1. Experimental Method. The direct observation of size specific bimetallic clusters requires a cluster source.[35] A laser vaporization (LaVa) source was used in this study, where a custom-made stainless steel system allowed the use of an external motor and the connection to a constant flow. The expansion nozzle was made of a Teflon tube (a length at 2.5 cm) with an inner diameter of 0.32 cm. Using the Hagen Poiseuille law, the conductance of the expansion nozzle can be estimated and was found to typically exhibit viscous flow. High-purity helium (Praxair, Inc., purity >99.995%) was used as buffer gas. The pressure inside the source during operating conditions was kept at ∼40 Torr, which suggests a Knudsen number of $\sim 2.8 \times 10^{-3}$ and a terminal Mach number of ∼12.3. The Al−Mg rod (50% Al−50% Mg, 6-mm diameter) was obtained from Kurt J. Lesker Co. The helium gas introduced from the inlet at the LaVa source carried the clusters through an adjustable iris into a flow tube where they encountered and reacted with O_2 at room temperature. The oxygen gas was introduced in the cluster beam ∼30 cm downstream from the source and allowed to react with the $Al_nMg_m^-$ clusters over a 60-cm distance and a time of ∼8 ms. The products were then extracted into a differentially pumped ion guide vacuum system, and analyzed via a quadrupole mass spectrometer (Extrel QMS). The pressure in the reaction flow-tube was at ∼0.7 Torr; that is, the number of collision for the clusters and reactant could be up to several hundred.

2.2. Computational Method. The electronic structures of the $Al_nMg_m^-$ clusters were probed using the first-principles molecular orbital approach wherein the cluster wave function is expressed as a linear combination of atomic orbitals located at the atomic sites. The exchange and correlation effects are included within generalized gradient density functional theory formalism. The actual calculations were carried out using the deMon2k code.[36] For exchange and correlation functional, we have used a generalized gradient approximation as proposed by Perdew, Burke, and Ernzerhof.[37] The aluminum and magnesium atoms are described using a DZVP basis set. The auxiliary density was expanded in primitive Hermite Gaussian functions by using the GEN-A2* auxiliary function set.[38] Previous investigations have been performed on the geometry and properties of pure metal clusters such as $Al_n^-/Al_n/Al_n^+$ and Mg_n/Mg_n^+;[39−44] however, the $Al_nMg_m^-$ alloy clusters have only been investigated at small sizes.[45] To determine the geometry and spin multiplicity of the ground state, the configuration space was sampled by running a genetic algorithm with a Gupta potential, and these initial configurations were then optimized employing the quasi-Newton Levenberg−Marquardt method.[46] All structures were fully optimized in delocalized redundant coordinates without imposing any symmetry constrains to allow for full variational freedom. Molecular orbitals were assigned subshells based on the symmetry of the molecular orbital and by inspecting the nodes of the wave function. The above analysis resulted in a clear assignment of nearly all molecular orbitals.

3. RESULTS AND DISCUSSION

In this study, experiments were performed to observe the size distribution of $Al_nMg_m^-$ cluster species on the basis of mass spectrometry. Figure 1a presents a mass spectrum of the obtained $Al_nMg_m^-$ clusters ($5 \le n \le 20$, $0 \le m \le 5$). Although the Al−Mg alloy rod used in the LaVa source has a composition of 50% Al and 50% Mg, the observed $Al_nMg_m^-$ cluster anions tend to contain significantly more Al atoms than Mg in the clusters; also abundant Al_n^- peaks were observed but no pure Mg_n^- cluster anions. This is due to the electronic properties of the alkali-earth metal (Mg: $[Ne]3s^2$), and Mg_2 has a low binding energy of 0.15 eV, making it a van der Waals molecule; in comparison, aluminum dimers form much more readily. Although metallic bonding emerges as multiple magnesium atoms are brought together, the difficulty of forming the Mg dimer and the much lower binding energies

dx.doi.org/10.1021/ja310467n | J. Am. Chem. Soc. 2013, 135, 4307−4313

of Mg-to-Mg than Mg-to-Al account for the absence of pure Mg_n^- clusters.[41] Figure 1b shows three-dimensional histograms of the integral signal intensities of the observed $Al_nMg_m^-$ cluster anions. In addition to Al_n^-, the dominant peaks belong to $Al_nMg_2^-$ and $Al_nMg_3^-$ series, such as $Al_5Mg_2^-$, $Al_9Mg_3^-$, $Al_{11}Mg_2^-/Al_{11}Mg_3^-$, $Al_{14}Mg_2^-/Al_{14}Mg_3^-$, $Al_{15}Mg_2^-/Al_{15}Mg_3^-$, $Al_{16}Mg_2^-$, and $Al_{17}Mg_2^-/Al_{17}Mg_3^-$. Also observed are several $Al_nMg_4^-$ and $Al_nMg_5^-$ series, etc.

In order to determine the chemical stability of the $Al_nMg_m^-$ clusters, we have studied the reaction with oxygen to examine their resistance to oxygen etching.[2−4] Figure 2 presents the

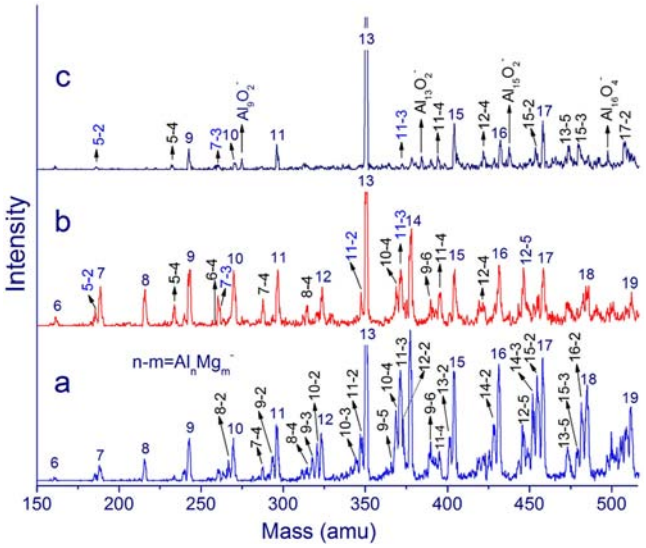

Figure 2. Nascent distribution of Al_n^- and $Al_nMg_m^-$ (a). Oxygen-etched distribution at different flow rate of the oxygen gas (b, 0.5 sccm; c, 6.8 sccm), where the peaks marked as n and $n-m$ correspond to Al_n^- and $Al_nMg_m^-$ clusters, respectively.

mass spectra showing the distribution of $Al_nMg_m^-$ species in the absence and presence of different flow rates of oxygen. Comparing with the nascent uniform distribution of $Al_nMg_m^-$ series (Figure 2a), the reaction with oxygen alters the mass spectra (Figure 2b,c). Even at a small flow rate of oxygen (0.5 sccm) as shown in Figure 2b, all the bigger clusters with $n > 13$ (both Al_n^- and $Al_nMg_m^-$) decrease in their intensity, but the relative intensity of Al_{13}^- is enhanced, as well as a few smaller peaks such as Al_{11}^- and Al_9^-, due to the fragmentation of larger clusters.[5] In comparison, when introducing a relatively large flow rate of the oxygen, most of the $Al_nMg_m^-$ are absent with only a few fragmentary peaks being observed (Figure 2c), indicating weak resistance to O_2 etching for nearly all of the $Al_nMg_m^-$ species ($1 \le m \le 6$). In addition, there are a few $Al_nO_x^-$ products being observed, such as $Al_9O_2^-$ and $Al_{15}O_2^-$ in the case of large flow rate oxygen; also, a few other peaks are observed having masses that correspond to species that could be either $Al_nMg_4^-$ or $Al_{n+3}O^-/Al_nO_6^-$. As the number of configurations for the alloy clusters $Al_nMg_m^-$ also increases substantially with the number of aluminum and magnesium atoms, our following studies are focused only on clusters containing up to 15 atoms and limited to clusters containing up to 3 Mg atoms.

These experimental observations suggest that $Al_nMg_m^-$ species are more reactive than pure Al_n^- clusters with oxygen, that is, the addition of Mg atoms enhances the combustion of pure aluminum clusters. However, $Al_nMg_m^-$ clusters with partial oxygen resistance are observed with noticeable intensity in the presence of small oxygen flow rates. For clusters containing 2 Mg atoms, only $Al_5Mg_2^-$ and $Al_{11}Mg_2^-$ appear with appreciable intensity. $Al_5Mg_2^-$ increases in intensity, while the intensity of $Al_{11}Mg_2^-$ slightly decreases with low oxygen flow. Both of these clusters are still observable with a high flow rate of oxygen, although their intensity is significantly decreased. Among the clusters containing 3 Mg atoms, $Al_7Mg_3^-$ and $Al_{11}Mg_3^-$ show prominent peaks at low oxygen flow rates, and remain detectable with a high flow in Figure 2c. Note that $Al_5Mg_2^-$ and $Al_{11}Mg_3^-$ correspond to 20 and 40 valence electrons and their stability could be rationalized within a confined nearly free electron model. However, $Al_7Mg_3^-$ and $Al_{11}Mg_2^-$ correspond to 28 and 38 valence electrons and their stability cannot be understood with a spherical jellium picture. Also, $Al_9Mg_3^-$ has 34 valence electrons that correspond to a closed shell in the jellium picture, and it is etched away at the presence of oxygen. Further, a few $Al_nMg_m^-$ clusters with 4 magnesium atoms are also observed after adding oxygen, but it is difficult to make definitive assignments as this series has masses virtually identical with oxide species.

To understand the observed variations in $Al_nMg_m^-$ clusters in the presence and absence of O_2, we have first undertaken theoretical studies to examine the ground state geometries and electronic structures of these species. For each size and composition, we generated a large number of atomic structures using a genetic algorithm and the structures were minimized by moving atoms in the direction of forces till the forces dropped below a threshold value of 4.5×10^{-4} au. The optimized minimum-energy structures of these $Al_nMg_m^-$ clusters are displayed in Figure 3 (details of absolute energies and coordinates are provided in the Supporting Information). The

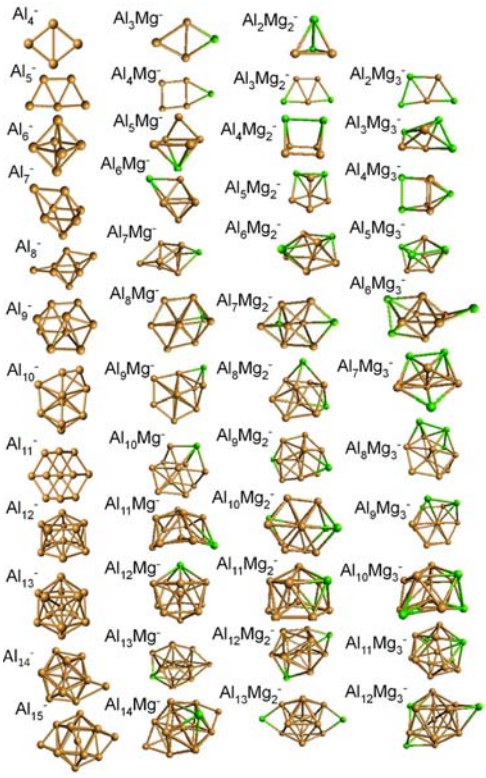

Figure 3. Optimized minimum-energy structures of the $Al_nMg_m^-$ clusters ($4 \le n+m \le 15$; $0 \le m \le 3$).

dx.doi.org/10.1021/ja310467n | J. Am. Chem. Soc. 2013, 135, 4307−4313

ground-state geometries of the small $Al_nMg_m^-$ clusters up to 5 atoms are found to follow planar or quasi-planar structures with rare exceptions, while all the bigger ones ($n+m \geq 6$) turn out to be three-dimensional. This progression of geometric changes beginning with 6 atoms resembles the monovalent species such as Na clusters, planar at small sizes and transforming to three-dimensional at bigger sizes. It is notable that the Mg−Mg bond is weaker than Al−Al and Al−Mg bonds, but the Mg atoms do not segregate and prefer to bind to multiple Al atoms. The Al−Al and Al−Mg bond lengths range from 2.70 to 2.95 Å, respectively. Therefore, the addition of Mg atoms influences the geometries of the alloy clusters $Al_nMg_m^-$ in addition to simply modifying the valence electron count.

The experimental reactivity studies identify that several anionic clusters exhibit resistance to oxidation, including $Al_5Mg_2^-$, $Al_7Mg_3^-$, $Al_{11}Mg_2^-$, and $Al_{11}Mg_3^-$. Among them, $Al_5Mg_2^-$ and $Al_{11}Mg_3^-$ correspond to 20 and 40 valence electrons respectively, which aim at fully filled shells based on the confined NFEG model. Based on this, the stability of the other mentioned clusters are unexpected, as 28 and 38 valence electrons do not normally correspond to closed shells. An alkali cluster with 34 valence electrons does appear as a magic species, but the 1F and 2P orbitals in aluminum clusters are generally similar in energy hence preventing 34 from being a magic number. So what governs the stability of the mentioned $Al_nMg_m^-$ species?

In general, the cluster reactivity with oxygen involves a spin excitation for the clusters with even number of electrons, while the spin excitation energies are governed by the HOMO−LUMO gaps. In view of this, we have calculated the HOMO−LUMO gaps for the $Al_nMg_m^-$ series (m = 0, 1, 2, 3). As the number of valence electrons is the most important parameter for determining the reactivity of a cluster, we have plotted the HOMO−LUMO gaps as functions of the number of valence electrons, $N(e^-)$, as shown in Figure 4. (Supporting Information, Table S1.A, lists all the data.) The number of valence electrons for $Al_nMg_m^-$ is calculated by simply using

$$N(e^-) = 3n + 2m + 1 \quad (1)$$

It is important to note that $Al_5Mg_2^-$ and $Al_{11}Mg_3^-$ both display large HOMO−LUMO gaps at 1.54 and 1.52 eV, respectively, which are only slightly smaller than the HOMO−LUMO gap of the superatomic species Al_{13}^- (1.87 eV). In comparison, the HOMO−LUMO gap of $Al_9Mg_3^-$ (34 valence electrons) is 0.84 eV, indicating less stability than $Al_5Mg_2^-$ and $Al_{11}Mg_3^-$, which is supported by the experimental observation. Several other clusters have strikingly large HOMO−LUMO gaps, such as $Al_7Mg_3^-$, $Al_{11}Mg^-$, and $Al_{11}Mg_2^-$, whereas they have valence electron counts of 28, 36, and 38, respectively. We also note that $Al_7Mg_3^-$ and Al_9^- have the same valence electron count of 28, but the HOMO−LUMO gap for Al_9^- is much lower than for the alloy cluster $Al_7Mg_3^-$.

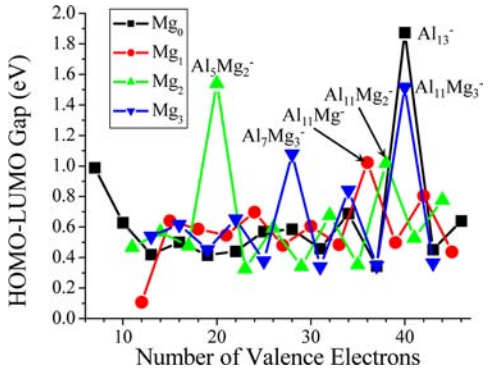

Figure 4. Calculated HOMO−LUMO gaps of $Al_nMg_m^-$ clusters plotted versus number of valence electrons.

In order to further probe the energetic stability of the $Al_nMg_m^-$ clusters, we have examined the energy loss by removing a Mg or an Al atom from the cluster, given by

$$\Delta E_{Mg} = -E(Al_nMg_m^-) + E(Al_nMg_{m-1}^-) + E(Mg) \quad (2)$$

$$\Delta E_{Al} = -E(Al_nMg_m^-) + E(Al_{n-1}Mg_m^-) + E(Al) \quad (3)$$

As results, Figure 5 shows the calculated ΔE_{Mg} and ΔE_{Al} as functions of the number of valence electrons. (Supporting Information, Table S2 tabulates the data.) Large values of ΔE_{Mg} and ΔE_{Al} correspond to the situation where there is a large loss of energy in removing a Mg or Al atom to form a smaller cluster; the peaks indicate energetic stability. The energy to remove a Mg atom is invariably smaller than the energy to remove an Al atom from the same $Al_nMg_m^-$ cluster. For all the three cluster series (m = 1, 2, 3), the removal energies display a range $0.4 < \Delta E_1 < 2.1$ eV for the removal of a Mg atom, while $2.0 < \Delta E_2 < 4.2$ eV for the removal of an Al atom. This could be the principle reason why all the observed $Al_nMg_m^-$ cluster series follow $m < n$.

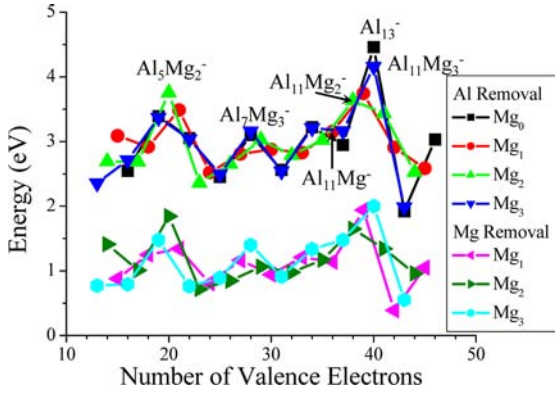

Figure 5. Calculated removal energies for Al and Mg atoms from the $Al_nMg_m^-$ clusters, where the black/blue, red/pink, and green/olive markers refer to the series with m = 1, 2, and 3, respectively. The horizontal axis is the number of valence electrons.

The results in Figure 5 show that the energetic stability of $Al_nMg_m^-$ clusters is maximized near the magic numbers of 20 and 40. The two most stable clusters in terms of Al removal energy are Al_{13}^- and $Al_{11}Mg_3^-$, both of which have 40 valence electrons. A second, slightly smaller peak in stability is observed at N = 20, with $Al_5Mg_2^-$ having the largest Al and Mg removal energy in this region. A smaller peak seems to appear with 28 valence electrons centered on $Al_7Mg_3^-$, which does not correspond to a magic number. Interestingly, the stability of clusters near the magic number seems to be also enhanced, $Al_{12}Mg^-$ with 39 valence electrons and $Al_{12}Mg_2^-$ with 41 valence electrons have quite large Al removal energies. Some of this reason may be due to the enhanced stability of clusters with icosahedral structures such as $Al_{12}Mg^-$; however, $Al_{12}Mg_2^-$ is not icosahedral and has an Al-removal energy higher than expected. A similar peak is observed around N = 20, suggesting

dx.doi.org/10.1021/ja310467n | J. Am. Chem. Soc. 2013, 135, 4307−4313

that the stability is enhanced as the number of valence electrons approaches a magic number.

The large HOMO−LUMO gaps and stability experimentally observed on $Al_5Mg_2^-$ and $Al_{11}Mg_3^-$ can be rationalized within a jellium model since the 20 and 40 electron configurations correspond to a filled electronic shell.[47] To further demonstrate it, we analyzed the molecular orbitals of these clusters. The molecular orbitals of $Al_5Mg_2^-$ and $Al_{11}Mg_3^-$ cluster are shown in Figure 6, along with the canonical closed electronic shell

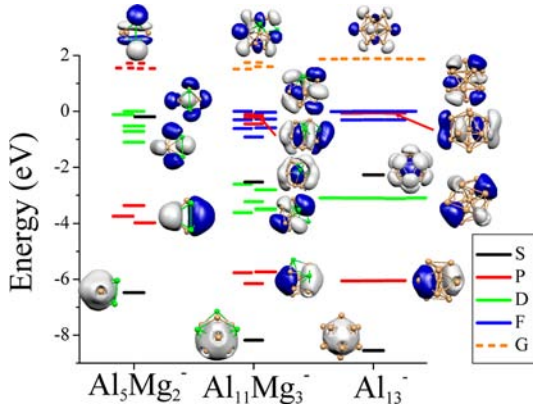

Figure 6. Molecular orbital diagrams of $Al_5Mg_2^-$, $Al_{11}Mg_3^-$, and Al_{13}^-.

cluster Al_{13}^-. We have labeled the molecular orbitals according to the assignment predicted by the spherical jellium model. The electronic structure of $Al_5Mg_2^-$ corresponds to $|1S^2|1P^6|1D^{10}2S^2\|2P^6|$, while $Al_{11}Mg_3^-$ corresponds to $|1S^2|1P^6|1D^{10}2S^2|2P^6|1F^{14}\|1G^{18}|$, in which the | indicates a large break in energies in the one electron orbitals while ‖ indicates the gap between filled and unfilled orbitals, and the uppercase letters refer to orbitals in a delocalized jellium model. We find that the electronic structures of these clusters agree well with the prediction of the jellium model, confirming that this is the origin of their stability.

Next, we consider the origin of stability in $Al_7Mg_3^-$ which is found to have unexpected resistance to oxygen etching as seen in Figure 2, and a large HOMO−LUMO gap as seen in Figure 4. It is surprising that both $Al_7Mg_3^-$ and Al_9^- have 28 valence electrons, but the alloy cluster has a markedly higher HOMO−LUMO gap. To examine this, we have plotted the molecular orbitals of $Al_7Mg_3^-$ and Al_9^- in Figure 7. Note that the structure of $Al_7Mg_3^-$ shows a significant deviation from the spherical shape. In such cases, the spherical jellium states can be split by the geometrical distortion of the cluster in a manner that can be regarded as a crystal-field-like splitting of delocalized orbitals. Based on this orbital diagram, the electronic structure of $Al_7Mg_3^-$ is best described as $|1S^2|2P^4|1P^2|1D^4|2S^2|1D^6|1F^4|2P^4\|$, in which the 1F and 2P levels are split by the geometry to a subshell, filling at 28 electrons with a HOMO−LUMO gap of 1.08 eV. In comparison, Al_9^- has a different structure due to the preference of small clusters toward an octahedral core; this structure results in a low-lying 1F orbital becoming the LUMO, and prevents the cluster from having an unusually large HOMO−LUMO gap.

As is shown in Figure 4, $Al_{11}Mg^-$ and $Al_{11}Mg_2^-$ also have large HOMO−LUMO gaps, and $Al_{11}Mg_2^-$ is resistant to oxygen etching despite having a nonmagic number of electrons at 38. $Al_{11}Mg^-$ is not observed in our experiments, so we are unable to draw any strong conclusion from this. To understand

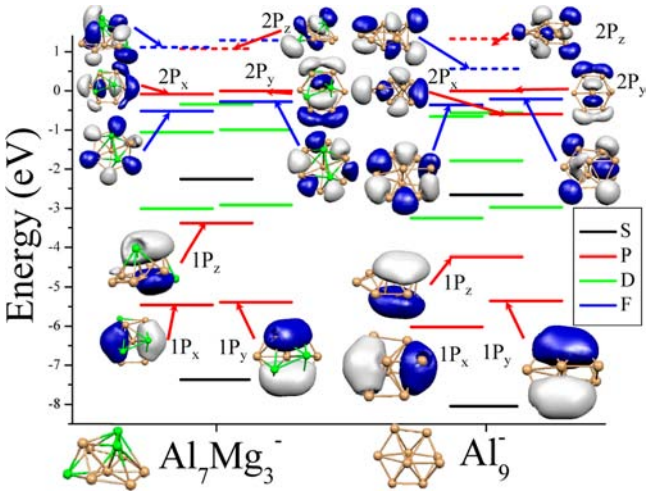

Figure 7. Molecular orbital diagrams of $Al_7Mg_3^-$ and Al_9^-.

the origin of stability of these clusters, we have also examined the molecular orbitals of $Al_{11}Mg^-$, $Al_{11}Mg_2^-$, and Al_{13}^+, as shown in Figure 8. Note that Al_{13}^+ also has 38 valence electrons

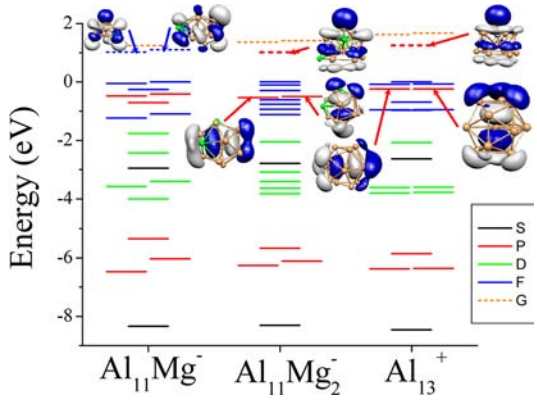

Figure 8. Molecular orbital diagrams of $Al_{11}Mg^-$, $Al_{11}Mg_2^-$ and Al_{13}^+.

and is known to have a large HOMO−LUMO gap through an oblate distortion which destabilizes a $2P_z$ orbital splitting the 2P subshell. In comparison, $Al_{11}Mg_2^-$ has virtually the same electronic structure as Al_{13}^+ and the $2P_z$ orbital also becomes the LUMO. Thus the electronic structure of $Al_{11}Mg_2^-$ is best described as $|1S^2|2P^6|1D^{10}1S^2|1F^{14}2P^4\|1P^2|1G^{18}|$. The reason why $Al_{11}Mg^-$ (36 valence electrons) has a large HOMO−LUMO gap is due to the crystal field splitting of a subshell. From the molecular orbital diagram (Figure 8), the electronic structure of $Al_{11}Mg^-$ is best described as $|1S^2|2P^6|1D^{10}1S^2|1F^{10}2P^6\|1F^4|1G^{18}|$. The structure of $Al_{11}Mg^-$ is even more oblate than $Al_{11}Mg_2^-$, and two sets of 1F orbitals are pushed up in energy, splitting the subshell. This is similar to the findings with the ellipsoidal jellium model that clusters having slightly fewer electrons than a magic number generally undergo oblate distortions akin to a Jahn−Teller distortion.

Finally, we would like to analyze the etching products of the $Al_nMg_m^-$ clusters after they are exposed to O_2. Figure 9 shows the energy released after the clusters react with O_2 following the two most likely processes,

$$Al_nMg_m^- + O_2 \rightarrow Al_{n-4}Mg_m^- + 2Al_2O \quad (4)$$

$$Al_nMg_m^- + O_2 \rightarrow Al_{n-3}Mg_{m-1}^- + Al_2O + AlMgO \quad (5)$$

dx.doi.org/10.1021/ja310467n | J. Am. Chem. Soc. 2013, 135, 4307−4313

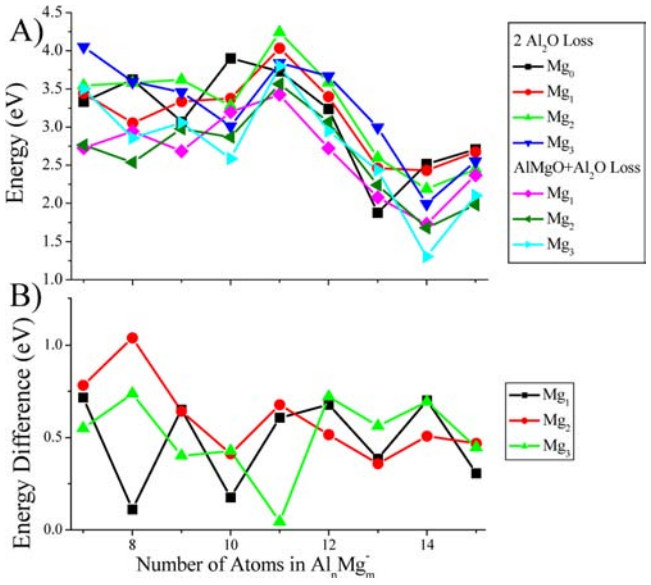

Figure 9. (A) Energy gain for removing two Al_2O molecules and a set of Al_2O and AlMgO molecules after the addition of O_2. (B) Energy difference for the loss of 4 Al atoms versus 3 Al atoms and 1 Mg atom after addition of O_2.

Figure 9A shows that all of these processes are exothermic, with Al_{13}^-, $Al_{11}Mg_3^-$, $Al_{12}Mg^-$, and $Al_{12}Mg_2^-$ having the lowest energy release, while $Al_9Mg_2^-$, $Al_{10}Mg^-$, and $Al_8Mg_3^-$ emit the most energy after the reaction with O_2. All the values in Figure 9B are greater than zero, indicating that these clusters studied release more energies by losing two Al_2O molecules rather than losing Al_2O and AlMgO simultaneously. This suggests that the reacting with O_2 may allow for an enrichment of Mg in $Al_nMg_m^-$ clusters. Both processes are exothermic, so it will be difficult to prevent some Mg from being removed off the cluster during the oxygen etching process.

4. CONCLUSIONS

We have investigated the stability of $Al_nMg_m^-$ alloy metal clusters anions which allows the sampling of virtually all valence electron counts from $N(e^-)$ = 11 to 46. This allows us to determine the magic numbers for Al-based metallic clusters, and to find clusters with enhanced stability with non-magic numbers. We observed $Al_nMg_m^-$ species and performed etching experiments with oxygen to screen for electronic shell closures. Theoretical studies determined the structures and origins of the clusters with large HOMO−LUMO gaps that control their reactivity with O_2. The species $Al_5Mg_2^-$ and $Al_{11}Mg_3^-$ were found to be quite stable versus other sizes due to electronic shell closures at 20 and 40 valence electrons. Unexpected stability was found for $Al_7Mg_3^-$, $Al_{11}Mg^-$, and $Al_{11}Mg_2^-$, which have valence electron counts of 28, 36, and 38, respectively, but do not correspond to the magic numbers from the spherical jellium model. The cluster stability was reconciled within a crystal field model which induces relatively large HOMO−LUMO gaps in metallic clusters by splitting subshells through a distortion of the geometry. This work has revealed the power and limitations of the spherical jellium model in alloy metal clusters.

■ ASSOCIATED CONTENT

Supporting Information

Tables for the theoretical results in Figures 4 and 5, and details of absolute energies and coordinates for the $Al_nMg_m^-$ clusters. This material is available free of charge via the Internet at http://pubs.acs.org.

■ AUTHOR INFORMATION

Corresponding Author

awc@psu.edu; snkhanna@vcu.edu

Author Contributions

[§]Z.L. and C.J.G. contributed equally to this work.

Notes

The authors declare no competing financial interest.

■ ACKNOWLEDGMENTS

This material is based upon work supported by the Air Force Office of Science Research under AFOSR Award No. FA9550-10-1-0071 (Z.L., A.W.C.) and through a MURI Grant Award No. FA9550-08-1-0400 (C.J.G., A.C.R., S.N.K.).

■ REFERENCES

(1) Li, H.; Meziani, M. J.; Lu, F.; Bunker, C. E.; Guliants, E. A.; Sun, Y.-P. *J. Phys. Chem. C* **2009**, *113*, 20539.
(2) Meziani, M. J.; Bunker, C. E.; Lu, F. L., H.; Wang, W.; Guliants, E. A.; Quinn, R. A.; Sun, Y.-P. *ACS Appl. Mater. Interf.* **2009**, *1*, 703.
(3) Huang, Y.; Risha, G. A.; Yang, V.; Yetter, R. A. *Combust. Flame* **2009**, *156*, 5.
(4) Romhanji, E.; Popovic, M. *Metalurgija* **2006**, *12*, 297.
(5) Leuchtner, R. E.; Harms, A. C.; Castleman, A. W., Jr. *J. Chem. Phys.* **1989**, *91*, 2753.
(6) Reber, A. C.; Khanna, S. N.; Roach, P. J.; Woodward, W. H.; Castleman, A. W., Jr. *J. Am. Chem. Soc.* **2007**, *129*, 16098.
(7) Schnoeckel, H.; Grubisic, A.; Li, X.; Stokes, S. T. *Science* **2008**, *319*, 438.
(8) Woodward, W. H.; Eyet, N.; Shuman, N. S.; Smith, J. C.; Viggiano, A. A.; Castleman, A. W. J. *J. Phys. Chem. C* **2011**, *115*, 9903.
(9) Reber, A. C.; Roach, P. J.; Woodward, W. H.; Khanna, S. N.; Castleman, A. W., Jr. *J. Phys. Chem. A* **2012**, *116*, 8085.
(10) Das, U.; Raghavachari, K. *J. Chem. Phys.* **2006**, *124*, 021101.
(11) Feyel, S.; Dobler, J.; Hoeckendorf, R.; Beyer, M. K.; Sauer, J.; Schwarz, H. *Angew. Chem., Int. Ed.* **2008**, *47*, 1946.
(12) Wang, Z.-C.; Dietl, N.; Kretschmer, R.; Ma, J.-B.; Weiske, T.; Schangen, M.; Schwarz, H. *Angew. Chem., Int. Ed.* **2012**, *51*, 3703.
(13) Roach, P. J.; Woodward, W. H.; Castleman, A. W., Jr.; Reber, A. C.; Khanna, S. N. *Science* **2009**, *323*, 492.
(14) Jellinek, J.; Acioli, P. H. *J. Phys. Chem. A* **2002**, *106*, 10919.
(15) Reber, A. C.; Khanna, S. N.; Castleman, A. W., Jr. *J. Am. Chem. Soc.* **2007**, *129*, 10189.
(16) Claridge, S. A.; Castleman, A. W., Jr.; Khanna, S. N.; Murray, C. B.; Sen, A.; Weiss, P. S. *ACS Nano* **2009**, *3*, 244.
(17) Knight, W. D.; Clemenger, K.; de Heer, W. A.; Saunders, M. Y.; Chou, M. Y.; Cohen, M. L. *Phys. Rev. Lett.* **1984**, *52*, 2141.
(18) Roach, P. J.; Woodward, W. H.; Reber, A. C.; Khanna, S. N.; Castleman, A. W., Jr. *Phys. Rev. B* **2010**, *81*, 195404.
(19) Clemenger, K. *Phys. Rev. B* **1985**, *32*, 1359.
(20) Hughbanks, T.; Rosenthal, G.; Corbett, J. D. *J. Am. Chem. Soc.* **1986**, *108*, 8289.
(21) Harms, A. C.; Leuchtner, R. E.; Sigsworth, S. W.; Castleman, A. W., Jr. *J. Am. Chem. Soc.* **1990**, *112*, 5673.
(22) March, N. H. *J. Mater. Sci. Technol.* **2001**, *17*, 581.
(23) Teo, B. K. *Abstr. Pap. Am. Chem. Soc.* **1984**, *188*, 106.
(24) Carlsson, A. E. *Phys. Rev. B* **1989**, *40*, 912.
(25) Dennler, S.; Morillo, J.; Pastor, G. M. *J. Phys. Condens. Mat.* **2004**, *16*, S2263.
(26) Zhu, L.; DePristo, A. E. *J. Catal.* **1997**, *167*, 400.

(27) Li, S. F.; Xue, X. L.; Jia, Y.; Zhao, G. F.; Zhang, M. F.; Gong, X. G. *Phys. Rev. B* **2006**, *73*, 165401.
(28) Janssens, E.; Neukermans, S.; Lievens, P. *Curr. Opin. Solid. State. Mater. Sci.* **2004**, *8*, 185.
(29) Medel, V. M.; Reveles, J. U.; Reber, A. C.; Khanna, S. N.; Castleman, A. W., Jr. *Phys. Rev. B* **2011**, *84*, 075435.
(30) Yamada, Y.; Castleman, A. W., Jr. *J. Chem. Phys.* **1992**, *97*, 4543.
(31) Castleman, A. W., Jr.; Khanna, S. N. *J. Phys. Chem. C* **2009**, *113*, 2664.
(32) Bergeron, D. E.; Roach, P. J.; Castleman, A. W., Jr.; Jones, N.; Khanna, S. N. *Science* **2005**, *307*, 231.
(33) Bergeron, D. E.; Castleman, A. W., Jr.; Morisato, T.; Khanna, S. N. *Science* **2004**, *304*, 84.
(34) Chaki, N. K.; Mandal, S.; Reber, A. C.; Qian, M.; Saavedra, H. M.; Weiss, P. S.; Khanna, S. N.; Sen, A. *ACS Nano* **2010**, *5*, 5813.
(35) de Heer, W. A. *Rev. Mod. Phys.* **1993**, *65*, 611.
(36) Köster, A. M.; Calaminici, P.; Casida, M. E.; Dominguez, V. D.; Flores-Moreno, R.; Geudtner, G.; Goursot, A.; Heine, T.; Ipatov, A.; Janetzko, F.; del Campo, J. M.; Reveles, J. U.; Vela, A.; Zuniga-Gutierrez, B.; Salahb, D. R. *deMon2k*; The deMon developers Cinvestav: Mexico City, 2006.
(37) Perdew, J. P.; Burke, K.; Enzerhof, M. *Phys. Rev. Lett.* **1996**, *77*, 3865.
(38) Calaminici, P.; Janetzko, F.; Köster, A. M.; Mejia-Olvera, R.; Zuniga-Gutierrez, B. *J. Chem. Phys.* **2007**, *126*, 044108.
(39) Sun, J.; Lu, W. C.; Wang, H.; Li, Z. S.; Sun, C. C. *J. Phys. Chem. A* **2006**, *110*, 2729.
(40) Durand, G. *J. Chem. Phys.* **1989**, *91*, 6225.
(41) Akola, J.; Manninen, M.; Hakkinen, H.; Land-man, U.; Li, X.; Wang, L. S. *Phys. Rev. B* **2000**, *62*, 13216.
(42) Sun, J.; Lu, W.; Li, C.; Wang, C. Z.; Ho, K. M. *J. Chem. Phys.* **2008**, *129*, 014707.
(43) Aguado, A.; Lopez, J. M. *J. Chem. Phys.* **2009**, *130*, 064704.
(44) Drebov, N.; Ahlrichs, R. *J. Chem. Phys.* **2010**, *132*, 164703.
(45) Reveles, J. U.; Köster, A. M. *J. Comput. Chem.* **2004**, *25*, 1109.
(46) Osorio, E.; Vasquez, A.; Florez, E.; Mondragon, F.; Donald, K. J.; Tiznado, W. *Phys. Chem. Chem. Phys.* **2013**, *15*, 2222.
(47) Knight, W. D.; Clemenger, K.; de Heer, W. A.; Saunder, W. A.; Chou, M. Y.; Cohen, M. L. *Phys. Rev. Lett.* **1984**, *52*, 2141.